CHLORITE/SMECTITE - ALKALI FELDSPAR METASOMATIC XENOLITHS FROM HYBLEAN MIOCENIC DIATREMES (SICILY, ITALY): EVIDENCE FOR EARLY INTERACTION BETWEEN HYDROTHERMAL BRINES AND ULTRAMAFIC/MAFIC ROCKS AT CRUSTAL LEVELS

Vittorio Scribano✉, **Salvatore Ioppolo** and **Paolo Censi**

Dipartimento di Scienze Geologiche, Università di Catania, Italy.
✉ *Corresponding author, e-mail: scribano@unict.it*

Keywords: *xenoliths, oceanic crust, hydrothermal brines, alkali feldspar, clay minerals, Hyblean Plateau. Sicily.*

ABSTRACT

Upper-Miocene tuff-breccia pipes from the Hyblean area (south-eastern Sicily) bear a number of ultramafic and mafic xenoliths (spinel-peridotites, pyroxenites, gabbroic rocks) whose study has led to conclude that the Meso-Caenozoic carbonatic and volcanic succession stands upon a fossil oceanic core-complex, probably connected with the adjacent Ionian crust.

Evidence for hydrothermal metasomatism is common in the Hyblean ultramafic and mafic xenoliths. In some cases, extreme metasomatic transformation and shearing have deleted original mineralogy and textures yielding unusual rocks, hereafter called "metasomatites". These rocks generally exhibit cataclastic texture, their hydrothermal mineral assemblage consisting of Na-rich alkali feldspar, chlorite/smectite (C/S) and/or smectite/illite (S/I) mixed layers, Fe-Ti oxide/hydroxide ± sieve-textured aegirine-augite ± titanite ± zircon. In addition, relics of Fo_{91} olivine, probably related to peridotite protoliths, rarely occur in these rocks. Comparing metasomatite whole chemistry to typical Hyblean oxide-gabbro, overall gain in H_2O, alkalis, HFSE, U, Th, HREE and significant loss in Ca and Mg are remarkable. The studied xenoliths probably represent fragments of deep-seated, mafic/ultramafic fault-breccia, recording the effects of long-lasting hypersaline hydrous fluids circulation in the Hyblean crustal basement.

INTRODUCTION

The Hyblean area (South-eastern Sicily, Italy) can be considered an uplifted, emerged portion of the Pelagian-Ionian foreland (Fig. 1a). The exposed stratigraphic sequence consists of Mesozoic-Caenozoic deep water carbonates and Neogene-Quaternary open-shelf clastics with several levels of basic volcanic rocks (Fig. 1b). The latter show either OIB either MORB affinity representing three main eruptive cycles (Late Cretaceous, Late Miocene and Plio-Pleistocene: e.g., Bianchi et al., 1987; Beccaluva et al., 1988). Dissected seamounts, with or without emerged tops, form the dominant volcanic structures in this region (Schminke et al., 1997).

Moreover, a few basaltic diatremes developed in the Late Miocene age (Carbone and Lentini, 1981). Hyblean diatremes exhibit a large number of deep-seated xenoliths (spinel-facies peridotites, pyroxenites, gabbroids: Scribano, 1987; Tonarini et al., 1996; Punturo et al., 2000; Sapienza and Scribano, 2000) whose study has finally led to conclude that the inaccessible crustal basement consists of a fossil oceanic core-complex. The latter is probably connected with the adjacent Ionian abyssal plain through a (fossil) transform margin, presently represented by the Malta Escarpment (Scribano et al., 2006 and references therein). The hypothesis that the lower crust beneath the Hyblean Plateau is of oceanic nature is supported by the following evidences: i) complete lack of *typical* continental crust rocks among the Hyblean xenoliths; ii) common occurrence of sheared oxide-gabbros, closely resembling those from modern (and fossil) oceanic fracture zones (Natland and Dick, 2001); iii) geophysical data (i.e. magnetometric, gravimetric: Arisi Rota and Fichera, 1987; Della Vedova et al., 1989) and, (iv) the lack of geochemical and isotopic evidence proving that the Hyblean volcanic rocks have suffered a continental crust contamination process (Trua et al., 1998; Bianchini et al., 1999).

The alteration degree of the Hyblean xenoliths is highly variable. Previous studies have dealt with the more fresh samples, as usual. Nevertheless, secondary minerals may be not the mere result of post depositional weathering: instead, they possibly record metasomatic processes started at deep crustal levels, prior to xenolith entrapment. Petrography and phase mineralogy of some remarkably altered xenoliths are reported here, aiming to infer their complex metasomatic history, hence to test their compatibility with an oceanic crust setting.

STUDIED SAMPLES

Hydrothermally modified xenoliths

Strongly serpentinized or carbonated peridotite xenolith are very common in any Miocenic tuff-breccia occurrences (Fig. 1b). In addition, gabbro xenoliths, especially the (dominant) sheared types, are affected by a wide range of alkaline and hydrous metasomatism which, usually, did not delete the original textures. Such mild to severe metasomatic transformations appear in form of albitization of plagioclase, replacement of primary mafic minerals by Na-amphiboles, aegirine augite, chlorites, smectites, Fe-oxi/hydroxes, widespread occurrence of zeolites, carbonates, K-feldspar. More rarely, mineralogical and textural changes have been so intense to obscure the nature of the protoliths yielding unusual rocks hereafter called "metasomatites". These can be divided in two main groups on the basis of silicate or carbonate dominant minerals. The silicate "metasomatite" xenoliths are the subject of this study.

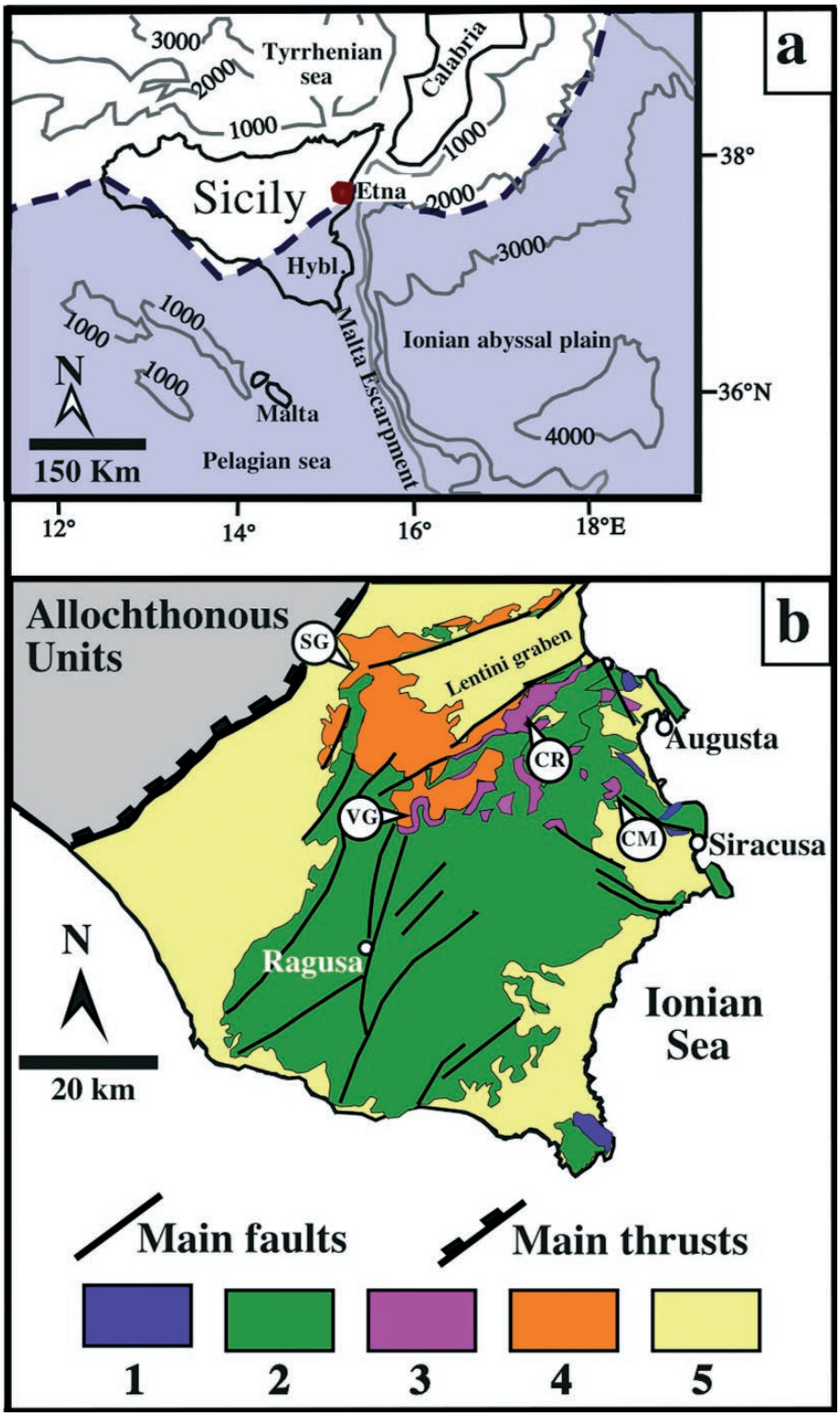

Fig. 1 - a) Map of Sicily and surroundings areas with essential bathymetry contouring (Hybl - Hyblean Plateau). Broken line broadly separates the Pelagian - Ionian foreland (shadowed area) from Maghrebian and Kabililo - Calabrian units (blank). b) Lithological sketch map of the Hyblean area with location of main xenolith occurrences (VG- Valle Guffari, CM- Cozzo Molino, CR- Carlentini, SG- Sigona Grande). 1- Meso-Caenozoic deep-water carbonates. 2- Upper Cretaceous OI-type basalts; 3- Upper Miocene basaltic tuff-breccia deposit. 4- Plio-Pleistocenic MOR-type basalts and OI-type basalts/basanitoids. 5- Neogene - Quaternary open shelf clastics.

Silicate "metasomatite" xenoliths

Silicate metasomatite xenoliths are common in the Hyblean tuff-breccia deposits, but samples larger than a few centimetres are rare, probably due to the intrinsic, friable nature of these rocks. This fact, coupled with their extreme textural and compositional heterogeneity, implies that one xenolith normally does not adequately represent the original deep-seated metasomatic rocks. Silicate "metasomatite" xenoliths generally show cataclastic texture, their mineral assemblages being largely dominated by Na-rich alkali feldspar and clay minerals. Fe-Ti oxides are ubiquitous in these rocks, whereas accessory quantity of aegirine-augite, titanite, zircon, forsteritic olivine, apatite, calcite and zeolites sometimes occur.

Sample FBZ from the Valle Guffari tuff-breccia deposits (Fig. 1b), in spite of its small size (≈ 4.5 x 3 cm), exhibits a good assortment of above mentioned minerals, hence it represents a suitable example for Hyblean metasomatites. This xenolith is composed of a roughly lenticular, relatively coarse-grained core (zone I) enfolded by a finer-grained, heavy sheared feldspatic - clayey matrix (zone II). Zone (I)

consists of aggregates of stubby, mortar-textured alkali feldspar grains tightly interlocked with dark, irregular, rounded-edged, hydrous-mafic small patches. The latter comprehend a vary textured assemblage of mafic clays and Fe-Ti oxide/hydroxides, rounded relics of sieve-textured aegirine-augite and ehuedral grains or crystal fragments of titanite (Figs. 2a, 2b, 2i). The boundary between mafic patches and host feldspar is marked by yellowish aggregates of clay minerals (Fig. 2a). Locally, two or more of these yellow rings join together, forming irregular clayey zones where sparse fractured zircon grains and their numerous rounded fragments are often immersed (Figs. 2h, 3a).

Zone (II) is composed of elongated areas of stretched alkali feldspar porphyroclasts with wide subgrain swarms, permeated by-, hence immersed in-, a pale coloured clayey matrix, forming altogether a pseudo-fluidal, near mylonitic,

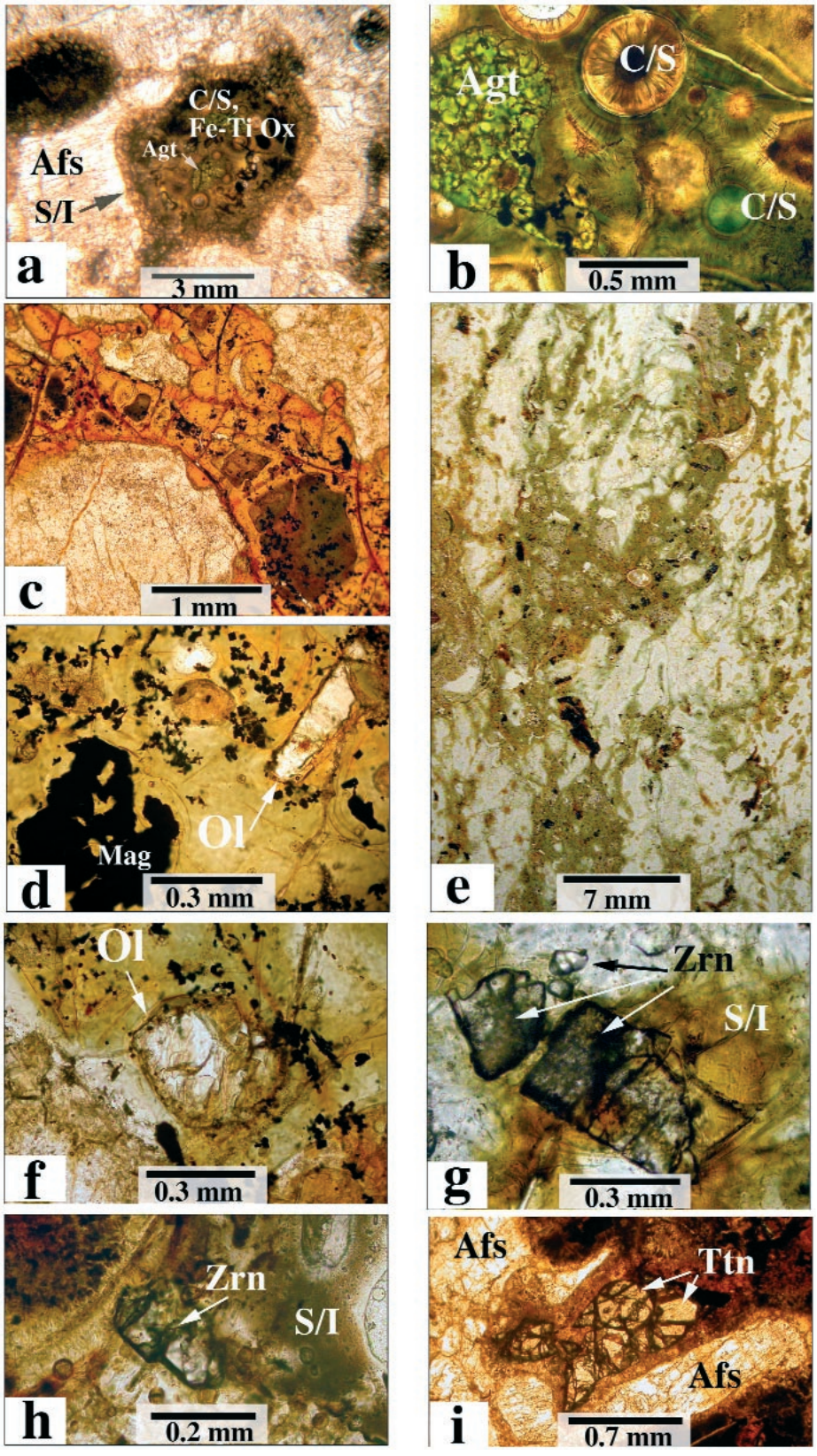

Fig. 2 - Plane polarized light microphotographs of different parts of metasomatite xenolith FBZ. a) Typical hydrous-mafic patch (dark brown) from the core zone (I) of the xenolith. A clayey rim (pale brown) separates this patch from surrounding alkali feldspar (Afs- alkali feldspar; S/I- smectite/illite mixed layers; Fe-ox- Fe-oxide/hydroxide; C/S- chlorite/smectite mixed layers. Other symbols after Kretz, 1983). b) Rounded, sieve-textured relic of aegirine-augite surrounded by vary textured mafic clays (C/S) inside one of above mentioned mafic patches (zone I). c) Alkali feldspar porphyroclast immersed in a turtle-shell textured clayey matrix from the sheared xenolith shell (zone II). d) Elongated relic of Mg-rich olivine from zone II; e) Scanner-acquired image of part of a thin section from zone (II): whitish areas represent alkali feldspar, greenish streaks mostly consist of clay minerals, dark patches are Fe-Ti oxide minerals. f) Rounded olivine relic immersed in a clayey matrix (zone II). g) Typical zircon grain and its rounded fragments from zone (II). h) Zircon grain immersed in the clayey corona of a hydrous-mafic patch from zone 1. I) Titanite micrograins set in a mafic-clayey matrix from zone I.

texture (Fig. 2e). These pale-coloured clayey areas are often cross cut by a complex set of micro-fractures, producing an irregular polygonal array. The polygon centres are always occupied by concentric shells of different clay minerals, outer rims consist of pale green or pale brown isotropic or near isotropic, probably colloidal, material. Sometimes these microfractures are marked by reddish iddingsite (Fig. 2c). Fe-Ti oxides are ubiquitous in these mesh-textured clayey areas, together with sparse, fractured zircon grains and their numerous, rounded fragments (Fig. 2g) and rare relics of Mg-rich olivine (Figs. 2d, 2f).

Other metasomatite xenoliths from Hyblean diatremes are less representative than above reported FBZ, since they do not contain one or more of the above mentioned mineralogical components. For istance, sample VB6 exhibits a coarse grained feldspatic core and a mylonitic clayey shell, closely similar to above described zone (II) of sample FBZ, whereas the hydrous-alkaline-mafic parts are missing. On the other hand some xenoliths (e.g. sample FB-A) consist of a millimetre-scale alternance of albite and mafic-clay layers. The latter host coarse ehuedral grains of titanite, tiny zircon fragments and sparse serpentinite shards.

ANALYTICAL METHODS

Mineral chemistry of the above mentioned FBZ metasomatite xenoliths was investigated by electron microprobe analyser (EMPA) Cameca Camebax Microbeam of the C.N.R. - Centro di Studi per la Geodinamica Alpina (Padova, Italy), equipped with four vertical WDS X-ray spectrometers and one EDS spectrometer. Total iron is reported as FeO. Synthetic oxides and minerals were used as standards. X-ray intensities were automatically corrected to oxide percent concentrations by PAP method. Prevention for loss of alkalis in alkali feldspar and other minerals was achieved by moving the stage slightly around during acquisition (analytical conditions: electron beam voltage = 15 kV and current = 10 nA, counting times set to 10 sec for both peak and background). Additional analyses were performed using a

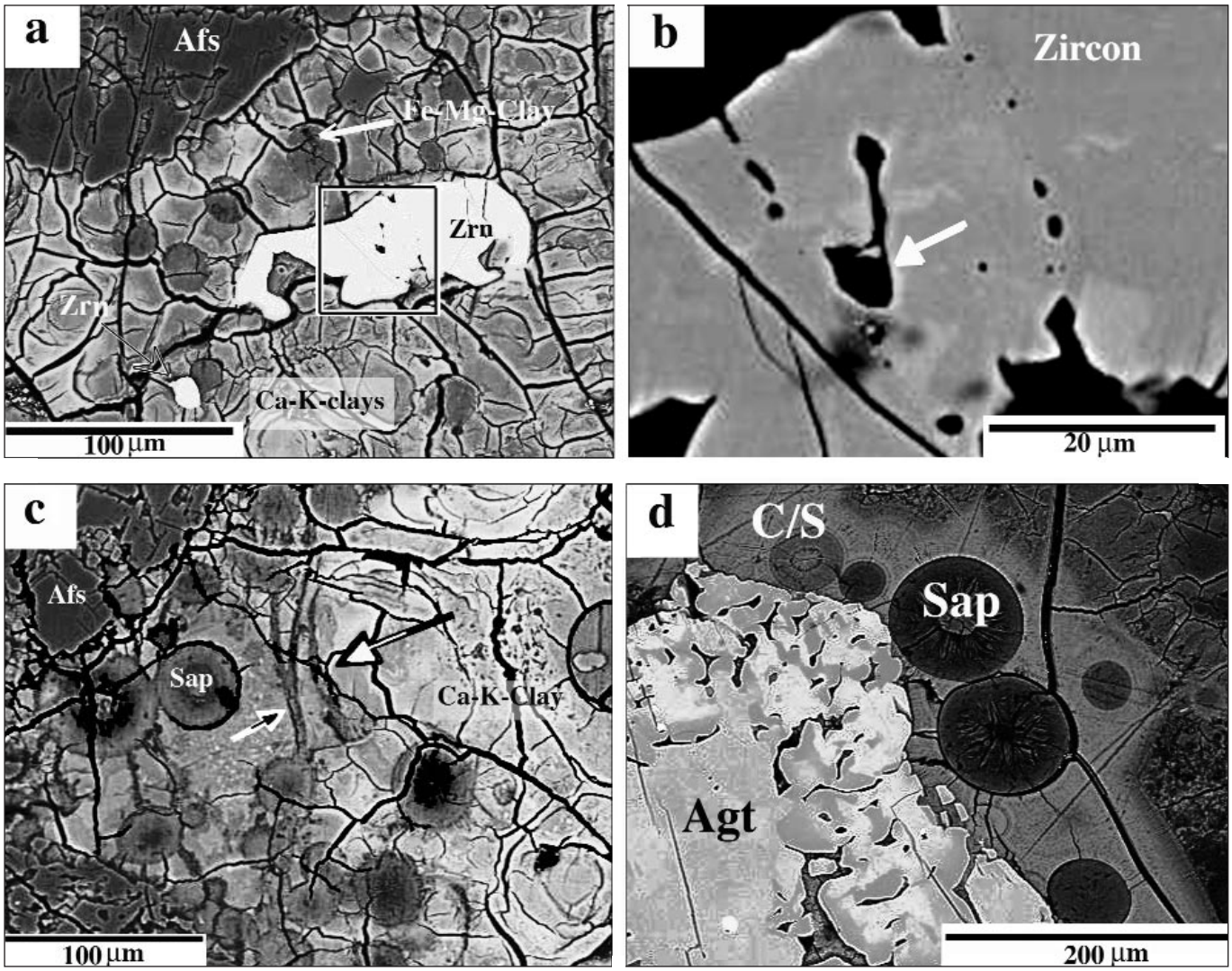

Fig. 3 - SEM images showing some details from zone (I) of the FBZ metasomatite xenolith. a) zircon grain (white in the photo) with a little satellite fragment (pointed by arrow), immersed in a clayey medium. The medium-gray small circles consist of Al-saponite clays, whereas the pale-gray scales are saponite/glauconite mixed layers. . Dark grey areas represent alkali-feldspar (Afs). Other symbols for minerals following Kretz, 1983. b) Magnification of the outlined section of the same zircon grain. The improved contrast evidences some patchy zoning (whitish areas in the photo), empty pores (former fluid inclusions) and a relatively large inclusion (pointed by the arrow) of silicate material, akin to a clay mineral in composition. c) Clay minerals and alkali feldspar fragments. Note the saponite channels connecting different fibrous saponite globules. d) Part of an aegirine-augite relic enveloped by different clay minerals in a mafic patch from zone (I). The present sieve-textured rim and the clayey original ghost border are clearly visible (C/S- chlorite/smectite mixed layers; Sap- discrete Al-saponite: S/I- smectite/illite mixed layers).

"LEO" SEM fitted with an EDS (operating conditions: 20 kV, 20 nA, lifetime 100 s, PAP corrections) at the Istituto Nazionale di Geofisica e Vulcanologia - Catania. X-Ray diffraction (XRD) analyses on powdered whole-rock have been performed using a SIEMENS D-5000 automatic diffractometer at Dept. of Geological Sciences, University of Catania. Whole-rock analyses were performed at Service d'Analyse des Roches et des Mineraux (SARM) laboratories in Nancy, France. Major elements were obtained by Inductively Coupled Plasma Emission Spectrometry (ICP), trace elements by Inductively Coupled Plasma Mass Spectrometry (ICP-MS). CO2 was detected volumetrically. Total iron is reported as Fe_2O_3. One whole-rock analysis has been performed by XRF spectrometry using a Philips PW-1400 spectrometer for both major and trace elements, at Dept. of Geological Sciences, University of Catania.

RESULTS

Mineral compositions

Alkali feldspar consists of strongly deformed, albite porphyroclasts (Ab_{95-98} - Or_{1-4} - An_{0-3}) with wide, finely fragmented, neoblastic rims, probably due to fracturing after recrystallization. The latter exhibit an increase in Or component which never exceeds 25 mol% (Table 1) Porphyroclasts generally exhibit chessboard extinction. Elongated grains rarely show mechanically distorted Carlsbad and faint, very thin, pericline lamellae. XRD results on bulk–rock powders are consistent with a complete Al, Si ordering, hence low-temperature structural state of these alkali feldspars (e.g. sharp peaks at 3.19 Å, 3.21 Å, 6.54 Å: JCPDS, Mineral Powder Diffraction Files, 1980). The feldspar sheared zones are always permeated by a close array of phyllosilicate flakes (Figs. 3a, 3c).

Phyllosilicates. Mixed layers chlorite/smectite (C/S), discrete saponite (S), and smectite/illite mixtures (S/I) were identified from microprobe analyses. Formulae were calculated on the basis of 28 Ox for (C/S) and 22 Ox for (S) and (S/I), always assuming total iron as divalent (Tables 2, 3). Compositions of clay minerals from the mafic patches (see above) conform to mixed layers chlorite/smectite: Si is always higher than the highest value for discrete chlorites (= 6.25 cations/28 Ox: Bettison and Schiffman, 1988). Ca and K represent the dominant interlayer elements. Sum of interlayer cations varies from 0.20 to 0.45; Mg# (i.e. 100 Mg/(Mg + Fe^{2+} tot.) varies from 0.4 to 0.6. Plotting major non interlayer cations (= Si + Al + Mg + Fe) vs total Al, the analysed C/S fall near the middle point of the chlorite - saponite tie-line (Fig. 4a: cf. Fulignati et al., 1997 and references therein). The same diagram also discriminates Al-saponite/beidellite interlayers. Sum of main interlayer cations (Ca + Na + K) vs Si (a.p.f.u./28 Ox) also show the chlorite/smectite interlayered nature of the studied clays. All plots evidence two groups with different C/S ratios (Fig. 4b).

On the other hand, the diagram of K vs tetrahedral Al puts into evidence smectite/illite (glauconite) interlayers (Fig. 5: see D'Antonio and Kristensen, 2005 and references therein). These clays exhibit elevated content in K_2O (= 4.5-5 wt%), CaO (= 5-6.5 wt%), low FeO and MgO. More interestingly, these clay minerals exhibit significant amount of Ba and Sr (Table 3, anls. 15-18), likely substituting K and Ca, respectively, in X site. XRD analyses on diverse whole rock powders show d_{001} = 15.5 Å with wide, uneven peak suggesting the occurrence of random interlayers. On the contrary, no mica peak (≈10 Å) has been detected.

Detailed SEM observations on FBZ clay minerals evidence the vary texture nature of C/S, the generally globular

Table 1 - Representative microprobe analyses (WDS) of alkali feldspar from metasomatite xenolith FBZ (P= porphyroclast; S= periphery subgrain).

	ALKALI FELDSPAR				
	1	2	3	4	5
wt%	P	P	P	S	S
SiO_2	69.14	69.31	69.60	69.45	67.23
Al_2O_3	19.35	19.65	19.01	19.12	21.33
TiO_2	0.00	0.00	0.01	0.00	0.00
FeO*	0.26	0.07	0.19	0.11	0.28
MnO	0.03	0.00	0.02	0.07	0.00
MgO	0.00	0.01	0.00	0.00	0.00
CaO	0.13	0.20	0.02	0.40	0.35
Na_2O	10.97	11.18	11.46	9.01	7.87
K_2O	0.63	0.29	0.28	2.83	3.23
Total	100.52	100.71	100.59	100.99	100.29
mol%					
Ab	95	97	98	81	77
Or	4	2	1.5	16	22
An	1	1	0.5	3	1

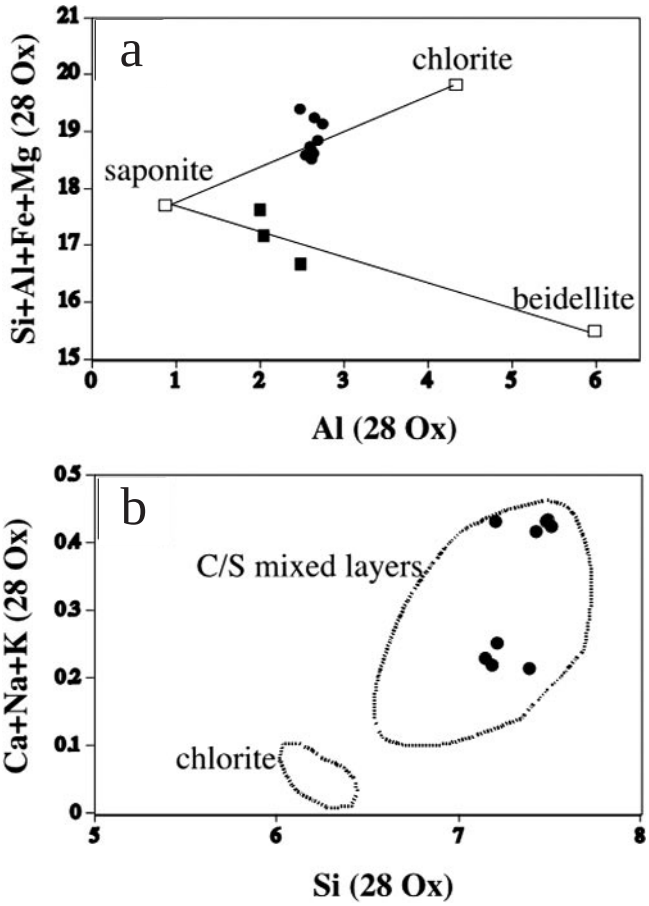

Fig. 4 - Discriminating diagrams (after Fulignati et al., 1997) for clay minerals from zone II (circles) and zone I (squares) of FBZ metasomatite xenolith. Formulae were calculated on 28 Oxygen equivalents basis. a) Diagram based on the sum of major non interlayer cations (Si + Al + Fe + Mg) vs total Al (a.p.u.f.- atoms per unit formula). b) Diagram based on the sum of major interlayer cations (Ca + K+ Na) vs Si a.p.u.f.

Table 2 - Representative microprobe analyses of mafic clays from zone (I) of xenolith FBZ.

	CLAY MINERALS (Oxygen equivalents = 28) Chlorite/Smectite mixed layers								
Anl#	6	7	8*	9	10*	11	12	13*	14*
wt%									
SiO_2	36.80	35.21	36.78	35.51	35.38	34.95	36.60	36.79	35.30
Al_2O_3	10.58	10.95	12.58	11.47	12.08	11.14	11.07	12.63	11.92
TiO_2	0.94	0.08	0.68	0.08	0.49	0.47	1.19	0.75	0.40
Cr_2O_3	0.03	0.00	nd	0.00	nd	0.05	0.00	nd	nd
FeO*	23.61	21.72	18.00	22.97	21.64	23.01	20.72	17.86	21.21
MnO	0.14	0.19	0.00	0.24	0.00	0.22	0.00	0.00	0.00
MgO	15.20	18.96	17.86	17.59	15.39	16.40	17.41	17.73	14.87
CaO	0.92	0.67	0.7	0.64	1.27	1.10	0.79	0.75	1.26
Na_2O	0.11	0.04	0.00	0.14	0.00	0.12	0.07	0.13	0.00
K_2O	0.73	0.22	0.65	0.22	0.48	0.53	0.06	0.66	0.64
Total	89.06	88.04	87.25	88.86	86.73	87.99	87.91	87.31	85.62
A.p.u.f.									
Si	7.476	7.176	7.374	7.205	7.308	7.203	7.384	7.371	7.380
Al IV	0.524	0.824	0.626	0.795	0.692	0.797	0.616	0.629	0.620
Al VI	2.009	1.806	2.346	1.948	2.249	1.909	2.016	2.353	2.317
Ti	0.144	0.012	0.102	0.012	0.076	0.073	0.181	0.113	0.063
Cr	0.005	0.000	-	0.000	-	0.008	0.000	-	-
Fe	4.011	3.702	3.017	3.897	3.738	3.965	3.496	2.992	3.708
Mn	0.024	0.033	0.000	0.041	0.000	0.038	0.000	0.000	0.000
Mg	4.603	5.760	5.337	5.319	4.738	5.038	5.235	5.295	4.634
Ca	0.200	0.146	0.151	0.139	0.281	0.243	0.171	0.161	0.282
Na	0.043	0.016	0.000	0.055	0.000	0.048	0.028	0.051	0.000
K	0.189	0.058	0.065	0.057	0.127	0.140	0.016	0.169	0.171
Σ cat.	19.228	19.533	19.120	19.468	19.209	19.462	19.142	19.133	19.174
Mg#	0.53	0.60	0.63	0.42	0.56	0.44	0.40	0.63	0.55

The asterisk (*) close to the analysis number (Anl#) denotes EDS method, other analyses have been obtained by WDS. All analyses were calculated on the basis of 28 Oxygen equivalents. Mg# = Mg/(Mg + Fe*); Fe has been assumed as total divalent (FeO*).

and fibrous occurrence of saponite, also forming braided narrow channels throughout the clayey zones, and the flat pattern of Fe-beidellite/illite mixtures (Figs. 3c, 3d).

Aegirine augite occurs as rounded, sieve-textured relics inside the above mentioned hydrous-mafic pools (Figs. 2b, 3d). It appears strongly pleochroic: X = leaf green, Y ≈ Z = yellowish green. Microprobe analyses evidence irregular variations for the aegirine component, from 17 to 33 mol% (average of 14 point analyses = 23 mol%). Mg# varies from 0.47 to 0.63 (average of 14 anls. = 0.53). It must be remarked that less sodic compositions (i.e. Ca/Na higher than ≈ 3) necessitate some Fe^{3+} (= 0.016-0.037 a.p.f.u.), in addition to Si, Al and Ti, to achieve tetrahedron stoichiometry. Some representative spot analyses are reported in Table 4.

Zircon appears as stubby, highly fractured grains along with rounded fragments disseminated in the clayey zones (Figs. 2g, 2h, 3a, 3b). EMP (WDS) analyses (Table 5) show slight, irregular compositional zoning (SiO_2 = 31-32 wt%, ZrO_2 = 64-67 wt%, FeO = 0.3-1.8 wt%. A number of fluid and silicate inclusions sometimes give these zircons a cloudy appearance. No optically detectable zircon grains totally free of inclusions have been observed. Qualitative (EDS) analyses on silicate inclusions show compositions compatible with the above reported Ca-Sr-Ba-bearing glauconite/nontronite mixtures. No information on fluid inclusions is presently available. Zircon grains from a representative fragment of xenolith FBZ have been studied for U-Pb,

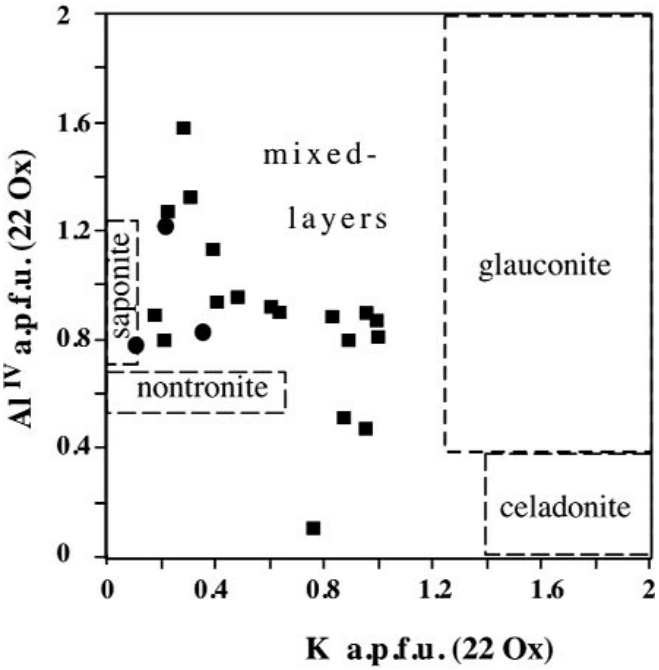

Fig. 5 - K vs Al(iv) apfu. plots for clay minerals from zone I (squares) and zone II (circles) of representative FBZ metasomatite xenolith. Formulae calculated on 22 Oxygen equivalents. Discriminating fields after D'Antonio and Kristensen (2005) and references therein.

Table 3 - Representative microprobe analyses of clay minerals from zone (II) of xenolith FBZ.

	CLAY MINERALS (Oxygen equivalents = 22)								
	Illite-rich mixed layers					Smectite-rich mixed layers			
Anl.#	15*	16*	17*	18*	19	20	21	22	23
wt%									
SiO_2	46.64	41.95	47.64	43.78	49.54	46.42	46.38	43.59	42.37
Al_2O_3	10.67	18.18	20.08	20.48	17.14	8.83	8.97	10.03	9.61
TiO_2	0.00	0.00	0.00	0.00	0.00	0.04	0.07	1.43	0.87
FeO*	0.43	3.19	0.40	0.46	0.75	10.62	9.67	20.52	23.52
MnO	0.00	0.00	0.00	0.00	0.01	0.02	0.12	0.00	0.00
MgO	0.00	1.13	0.21	0.42	0.17	18.09	18.05	6.45	6.88
CaO	6.34	5.30	5.46	6.22	4.64	1.22	1.45	1.06	0.92
Na_2O	0.36	0.25	0.33	0.16	0.61	0.00	0.07	0.42	0.38
K_2O	4.69	4.81	5.04	4.75	3.87	2.52	2.11	3.95	3.29
BaO	1.34	1.32	1.41	1.23	nd	nd	nd	nd	nd
SrO	0.6	0.97	0.97	0.91	nd	nd	nd	nd	nd
Total	80.07	77.10	81.54	78.41	76.80	87.76	86.95	87.45	87.84
A.p.u.f.									
Si	7.360	7.074	7.385	7.101	7.876	6.934	6.948	6.954	6.834
Al iv	0.640	0.926	0.615	0.899	0.124	1.066	1.052	1.046	1.116
Al vi	3.018	2.687	3.053	2.016	3.087	0.488	0.532	0.840	0.660
Ti	0.000	0.000	0.000	0.000	0.000	0.004	0.008	0.172	0.106
Fe	0.057	0.450	0.052	0.062	0.100	1.326	1.212	2.738	3.172
Mn	0.000	0.000	0.000	0.000	0.001	0.003	0.015	0.000	0.000
Mg	0.000	0.284	0.048	0.101	0.040	4.027	4.031	1.534	1.654
Ca	1.072	0.957	0.907	1.081	0.790	0.195	0.233	0.182	0.158
Na	0.110	0.082	0.099	0.051	0.188	0.001	0.021	0.130	0.118
K	0.944	1.034	0.997	0.982	0.785	0.480	0.403	0.804	0.676
Ba	0.083	0.087	0.086	0.078	-	-	-	-	-
Sr	0.055	0.095	0.087	0.086	-	-	-	-	-
Σ cations	13.339	13.677	13.328	12.457	13.001	14.525	14.461	14.398	14.546
Mg#		0.38	0.48	0.40	0.28	0.75	0.76	0.36	0.34

The asterisk (*) close to the analysis number (Anl#) denotes EDS method, other analyses have obtained by WDS. All analyses were calculated on the basis of 22 Oxygen equivalents. Fe has been assumed as total divalent (FeO*).

Table 4 - Representative microprobe analyses (WDS) of aegirine-augite relic from zone (I) of xenolith FBZ.

	AEGIRINE-AUGITE				
Anl#	24	25	26	27	28
wt%					
SiO_2	52.18	52.04	52.31	50.97	51.10
Al_2O_3	0.83	0.67	0.77	0.55	0.35
TiO_2	0.43	0.51	0.42	0.49	0.17
Cr_2O_3	0.00	0.00	0.00	0.05	0.00
FeO*	19.19	19.01	18.93	10.60	19.16
MnO	0.96	1.23	1.09	1.03	1.03
MgO	6.02	6.26	6.36	8.32	7.30
CaO	15.8	16.44	16.25	19.31	18.51
Na_2O	4.43	4.28	4.42	2.20	2.40
Total	99.84	100.44	100.55	101.21	100.77
mol%					
Di+Hd	65	67	65	82	81
Agt	33	32	33	18	19
Ts	2	1	2	0	0
Mg#	0.51	0.55	0.56	0.58	0.51

Di+Hd= Ca - Al(iv); Aeg= Na; Ts= Al(iv). Fe^{3+} has been estimated on stoichiometry basis.

Table 5 - Representative microprobe analyses (WDS) of zircon grains (Anl# 29, 30), titanite (Anl# 31) and isotrope material (Gel: Anl# 32) from zone (II) of FBZ metasomatite xenolith.

	ZIRCON		TITANITE	GEL
wt%	29	30	31	32
SiO_2	32.35	32.17	30.18	60.95
Al_2O_3	0.01	0.03	0.46	12.90
TiO_2	0.04	0.01	36.85	0.79
FeO*	1.83	1.14	2.28	7.31
MnO	0.00	0.00	0.15	0.53
MgO	0.00	0.03	0.00	1.52
CaO	0.03	0.07	26.59	2.06
Na_2O	0.00	0.00	0.46	0.88
K_2O	0.00	0.00	0.00	1.89
ZrO_2	65.74	66.47	nd	nd
Total	100.00	99.92	96.97	88.86

Lu-Hf isotope systematics by Sapienza et al. (2005a). Published preliminary results show that U-Pb ages for fifty-eight zircon grains scatter from 184 to 283 Ma, with ~ 72% data clustering around 245±9 Ma and lying close to Concordia. Five grains show scattered U-Pb ages from 1939 to 2687 Ma.

Titanite is a common mineral phase in the Hyblean silicate metasomatites. It occurs in the mafic patches from zone (I) as small euhedral grains or coarse, anhedral fragments. Other metasomatite xenoliths (e.g. sample FBA) exhibit coarse euhedral titanite crystals. Microprobe (WDS) analyses show a quite uniform composition. Low totals are probably due to some intracrystalline OH (Table 5, anl. 31). Composition of the gel-like material from zone (II) (see previous section) broadly approaches an illite/nontronite mixture, but with a significant excess of silica (Table 5, anl. 32).

Olivine occurs as tiny, either elongated or rounded relics (Figs. 2d, 2f) immersed in clay minerals. Some microprobe spots, relatively distant from the relic rim, show the highest magnesian composition (Fo_{91}), which probably records the protolith olivine. Iron dramatically increases towards the relic rim (Table 6).

Fe-Ti oxides, are ubiquitous in these metasomatite xenoliths, especially in sample FBZ. Relatively coarse Fe-Ti oxide grains exhibit irregular shape consisting of close intergrowths of magnetite, Ti-magnetite and ilmenite. Euhedral micrograins consist of magnetite and subordinate hematite.

Rare *apatite* micrograins are set only in the mafic patches from zone I, close to titanite grains.

Very rare *calcite* occurs as tiny ovoids immersed in the clayey material.

Whole-rock chemistry

Two fragments representing mylonitic shells of metasomatite xenoliths VB6 and FBZ have been analysed for major and trace elements. A fragment enriched in the core component (zone I) of xenolith FBZ has been also analysed by XRF for major and some trace elements. These analyses are reported in Table 7. Despite significant compositional differences between shell- and core-derived fragments,

Table 6 - Representative microprobe analyses (WDS) of olivine relic from FBZ xenolith (zone II).

	OLIVINE		
	Core	Rim(a)	Rim(b)
Anl#	33	34	35
wt%			
SiO_2	42.11	41.88	40.33
TiO_2	0.00	0.00	0.02
Cr_2O_3	0.00	0.00	0.02
FeO*	9.20	9.34	15.65
MnO	0.10	0.32	0.32
MgO	50.22	50.09	43.71
CaO	0.07	0.06	0.36
Total	101.70	101.69	100.41
mol%			
Forsterite	91	90	83
Fayalite	9	10	17

Table 7 - Representative whole rock analyses (major and some trace elements) of representative portions from two metasomatite xenoliths (VB6 and FBZ).

	METASOMATITE			OXIDE-GABBRO
	VB6-f	FBZ(II)	FBZ(I)	FB-f1
wt%				
SiO_2	57.66	54.82	51.98	36.40
TiO_2	0.46	0.41	0.79	5.40
Al_2O_3	16.10	16.11	15.79	10.00
Fe_2O_3	6.00	6.61	8.07	22.30
MnO	0.16	0.11	0.18	0.20
MgO	1.52	2.68	3.96	9.00
CaO	1.24	1.29	2.83	13.40
Na_2O	4.73	4.53	3.15	1.30
K_2O	4.72	3.42	3.59	0.10
P_2O_5	0.00	0.00	0.10	0.10
L.O.I.	7.34	9.93	9.51	1.00
Tot.	99.93	99.91	99.95	99.20
H_2O	*6.70*	*9.66*	*nd*	*0.90*
CO_2	*0.64*	*0.27*	*nd*	*0.10*
ppm				
La	25.5	18.4	24.3	4.5
Ce	56.1	35.5	81.5	17.4
Pr	6.5	3.7	nd	3.1
Nd	23.3	12.9	nd	19.3
Sm	4.7	2.4	nd	5.3
Eu	1.1	0.6	nd	1.9
Gd	3.9	1.9	nd	5.8
Tb	0.5	0.3	nd	0.7
Dy	3.5	2.2	nd	4.0
Ho	0.6	0.4	nd	0.7
Er	1.9	1.4	nd	1.8
Tm	0.3	0.2	nd	0.2
Yb	2.5	2.1	nd	1.3
Lu	0.5	0.4	nd	0.2
V	5.1	7.6	9.5	534.8
Cr	0.0	5.2	7.1	56.8
Co	1.7	2.5	1.2	61.7
Ni	12.8	60.8	25.8	60.3
Cu	0.0	0.0	nd	49.3
Zn	192	93.0	87.2	219.3
Sr	668	454	2454	1063.6
Rb	50.5	38.0	49.4	3.2
Ba	738	538	2797	83.8
Th	3.8	6.3	nd	0.0
Ta	5.0	5.2	nd	0.6
Nb	69.6	73.2	nd	7.0
Zr	511	639	277	59.8
Hf	12.5	15.6	nd	2.0
Y	15.6	10.9	12.2	20.6

VB6F= represents the sheared outer shell of xenolith VB6. FBZ(I) represents the inner zone of xenolith FBZ. FBZ(II) represents the outer shell of the same xenolith. n.d.= not detected. The chemical composition of a typical Hyblean oxide-gabbro xenolith (sample FB-f1, Scribano et al., 2006) has been also reported for comparisons. Analithical methods: major elements of VB6F, FB(II) and FB-F1: E-ICP; FBZ(I): XRF. Trace elements of VB6F, FB(II) and FB-F1: ICP-MS; FBZ(I): XRF.

overall metasomatite compositions display elevated alkalis (Na_2O = 3.1-4.5 wt%; K_2O = 3.4-4.7 wt%), H_2O (= 7-10 wt%) and relatively low CaO (=1.2-2.8 wt%), consistent with the high modal abundance of alkali feldspar and clay minerals. In addition, high Zr (up to 639 ppm), U (up to 1.48 ppm), Th (up to 6.39 ppm) are related to the disseminated zircon grains.

DISCUSSION

A prime goal of this study is to infer the nature of the metasomatite protolith(s). For this purpose, the relics of aegirine augite occuring in the hydrous-mafic patches from zone (I) of xenolith FBZ provide key information. Indeed, this mineral is very common in other Hyblean metasomatic xenoliths, whose texture and chemical composition testify a gabbroic *parentage*. Moreover, hydrothermal aegirine-augite is well known in diverse ophiolitic metagabbros, as well as those from the Italian Northern Apennines (e.g. Cortesogno and Lucchetti, 1984). Ca-Na- pyroxene is strongly out of equilibrium in the studied metasomatite, having been largely replaced by mafic clays (C/S mixed layers), probably representing retro-hydrothermal products after chlorite (Robinson et al., 2002).

We suggest a hydrothermal origin of titanite and zircon grains from the studied metasomatites. This hypothesis is in agreement with both experimental studies and natural evidences indicating that halogens-bearing hydrothermal fluids are capable to mobilize even highly "immobile" HFS elements, including Zr (e.g. Rubin et al., 1993; Kerrich and Kyser, 1994; Aja et al., 1995; Salvi and Williams-Jones, 1996; Hoskin et al., 1998; Geisler et al., 2002; Hoskin, 2005). In addition, recent studies reveal that hydrothermal clays and other hydrous minerals from brine-saturated oceanic crust contain significant quantity of Zr (Plank and Langmuir, 1998; Lassiter et al., 2002; Boschi et al., 2005). Moreover, hydrothermal zircon and unusual Zr-bearing mineral phases (e.g: $Sr_3Na_2Zr(CO_3)_6 \cdot 3H_2O$, weloganite) have been reported from fossil oceanic crust occurrences (e.g. Sudetic ophiolite: Dubinska et al., 2004).

The high modal abundance of zircon in the studied "metasomatite" (more than 100 grains have been extracted from a 2 cm fragment of xenolith FBZ: Sapienza et al., 2005b) also support the hydrothermal origin of this mineral (Pettke et al., 2005). Moreover, silicate inclusions from the studied zircon grains suggest that they have crystallized in a clayey medium, (see previous section and Fig. 3b). Nevertheless, even admitting that a few zircon grains from the FBZ metasomatite record an early magmatic source, this would not be in contrast with the oceanic origin of the studied rock, since igneous zircons have been found in different oceanic settings (e.g. Cannat et al., 1997; Brunelli et al., 2005).

Olivine represents another important relic mineral from the metasomatite xenolith. The Mg-rich composition (Fo_{91}) of this mineral conforms with olivines from Hyblean mantle peridotites (e.g. Scribano, 1987). This fact, coupled with the occurrence of mesh-like textures, suggests that the studied metasomatite consists of mingled fragments of strongly altered peridotite and gabbro.

Whole rock composition of a typical, relatively fresh (L.O.I. = 1 wt%), Hyblean oxide-gabbro xenolith (sample FB-f1: Scribano et al., 2006) has been selected to compare with studied metasomatite compositions (Table 7). Fig. 6 shows that metasomatites have had overall gain in H_2O, alkalis, HFSE, U, Th, HREE and significant loss in Ca, Mg, Fe (Mg > Fe) and MREE. In particular, the enrichment in Na is primarily due to secondary alkali feldspar with subordinate contribution by Na-pyroxene and clay minerals. The latter generally represent the most important depositors for K, though K-feldspar veinlets cross-cutting albite porphyroclasts have been observed in some Hyblean metasomatites (e.g. xenolith VB6: Scribano et al., 2003). On the other hand, the released Ca and Mg can account for the occur-

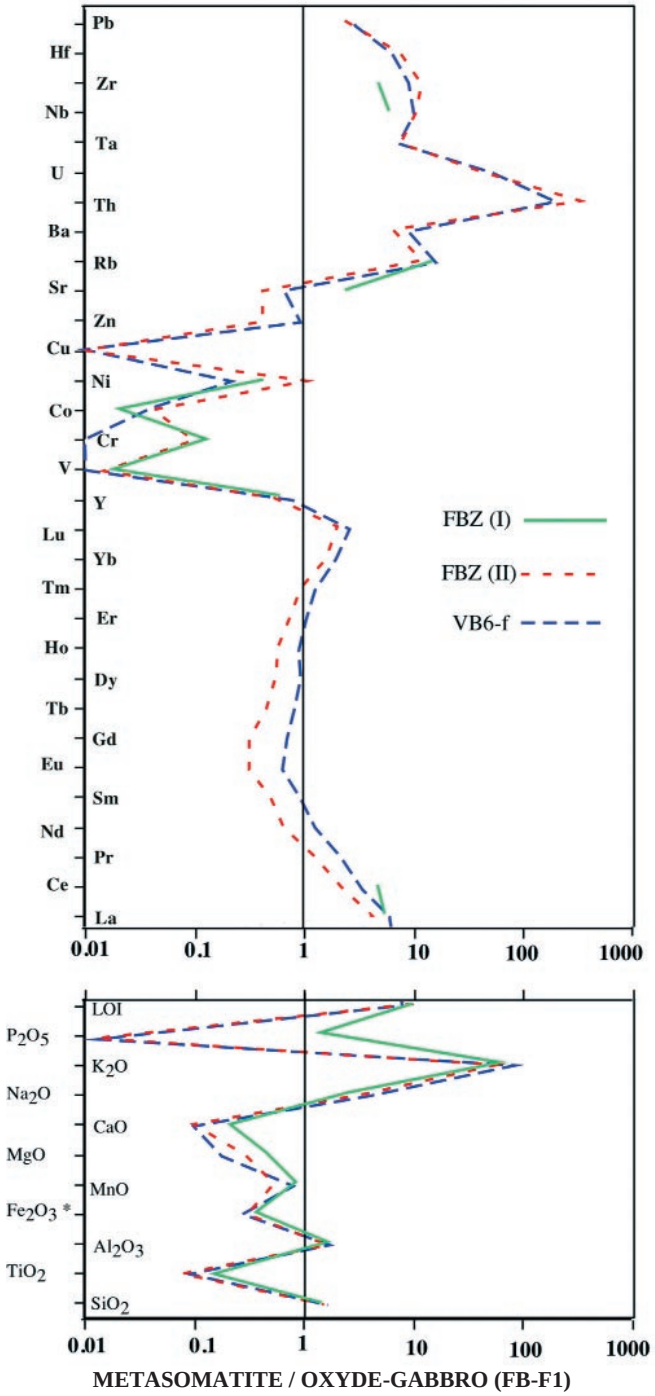

Fig. 6 - Whole-rock chemical compositions (major and some trace elements) of studied metasomatite xenolith normalized to a typical Hyblean oxide-gabbro xenolith (sample FB-f1: Scribano et al., 2006). FBZ (I) is a fragment of FBZ xenolith enriched in the zone (I) component. FBZ (II) well represents the sheared outer shell. VB6-f represents the mylonitic shell of metasomatite xenolith VB6.

rence of ophicarbonate xenoliths (dominant calcite + saponite + talc+ chalcedony ± albite ± enstatite, ± Cr-diopside: Scribano, unpublished data).

Some inference on the fossil hydrothermal system derives from the textures of Hyblean metasomatite xenoliths. Cataclastic to mylonitic textures imply a tectonically controlled hydrothermal system. Moreover, tectonic fracturing and hydrothermal circulation are closely allied, since different specific volume between fresh protolith (e.g. peridotite) and its hydrous counterpart (e.g. serpentinite) gives brittle deformations at diverse scales. Assuming the crustal model proposed by Scribano et al. (2006), sea-floor exposure of the top of a highly fractured gabbro-peridotite ridge represents an appropriate scenery for a seawater dominated hydrothermal system.

Published data (Aja et al., 1995; Salvi and Williams-Jones, 1996; Palandri and Reed, 2003) suggest that reaction between seawater and basalt (gabbro) at about 300 °C decreases the pH from neutral to quite acid (= 3.8). Such acid fluids leach and mobilize base metals which may be transported through fault planes far away from the original gabbroic rock. In contrast, reaction of seawater with peridotite produces basic, hyperalkaline hydrothermal fluids. Mixing of these fluids with contrasting pH, or mixing of one of them with cold seawater, leads to formation of different authigenic hydrothermal minerals, either silicates or carbonates.

It is remarkable the close similarity of some textural and compositional aspects (i.e. cataclastic texture, occurrence of secondary alkali feldspar, chlorite/smectite interlayers, hydrothermal zircon) of the studied xenoliths with some metasomatites (blackwalls) occurring between rodingites and serpentinites in ophiolite massifs worldwide (e.g. Dubinska et al., 2004). Finally, the lack of discrete chlorite and the abundance of C/S and S/I clay minerals in the studied rocks are probably related to multistage hydrothermalism, with an overall decreasing temperature through time (Robinson et al., 2002).

CONCLUSIONS

The above data and discussion lead to the following conclusive remarks:

a) the studied metasomatite xenoliths represent fragments of deep-seated hydrothermal breccia recording the effects of long-lasting hypersaline hydrous fluids (brine) circulation throughout tectonized mafic/ultramafic rocks at crustal levels;

b) the development of a seawater dominated and tectonically controlled hydrothermal system in the Hyblean crustal basement supports the hypothesis of its fossil oceanic nature. The probable lithospheric continuity with the adjacent Ionian domain is consistent with published zircon ages assigning to Early Triassic the main hydrothermal event;

c) such deeply and broadly transformed crust should be taken into account for interpreting geochemical data of the Hyblean volcanic rocks. In fact, silicate liquids from brine-induced melting of altered oceanic crust and high-T hydrosaline solutions are considered very effective metasomatic agents (e.g. Lassiter et al., 2002).

ACKNOWLEDGEMENTS

Constructive reviews by L. Gaggero, A. Montanini, T. Trua were truly appreciated. Large part of this study has been funded by grant “Ex 60%, Università di Catania ” to V. S. We wish to thank L. Miraglia (INGV, Catania) and G. Malandrino (Dept. of Chemical Sciences, Catania University) for SEM guidance, and E. Giuffrida (Dept. of Geological Sciences, Catania University) for XRF assistance.

REFERENCES

Aja S.U., Wood S.A. and Williams-Jones A.E., 1995. The aqueous geochemistry of Zr and the solubility of some Zr-bearing minerals. Appl. Geochem., 10 (6): 603-620.

Arisi Rota F. and Fichera F., 1987. Magnetic interpretation related to geo-magnetic provinces:The italian case history. Tectonophysics, 138: 179-196

Beccaluva L., Siena F., Coltorti M., Di Grande A., Lo Giudice A., Macciotta G., Tassinari R. and Vaccaro C., 1998. Nephelinitic to tholeiitic magma generation in a transtentional tectonic setting: an integrated model for the Iblean volcanism, Sicily. J. Petrol., 39: 1547-1576

Bettison L.A. and Schiffman P., 1988. Compositional and structural variations of phyllosilicates from the Point Sal ophiolite, California. Am. Mineral., 73: 62-76.

Bianchi F., Carbone S., Grasso M., Invernizzi G., Lentini F., Longaretti G., Merlini S. and Mostardini F., 1987. Sicilia orientale: Profilo geologico Nebrodi - Iblei. Mem. Soc. Geol. It., 38:429-458.

Bianchini G., Bell K. and Vaccaro C., 1999. Mantle sources of the Cenozoic Iblean volcanism (SE Sicily, Italy): Sr-Nd-Pb isotopic constraints. Mineral. Petrol., 67: 213-222

Boschi C., Frueh-Green G., Karson J., Kelley D., Dini A. and Delacour A., 2005. Mass transfer and metasomatism during detachment faulting and development of an oceanic core complex (MAR 30° N). Epitome 1 (Geoitalia 2005): 24.

Brunelli D. and Onboard Scientific Parties, 2005. Cruise report expeditions 304 and 305: drilling the oceanic core complex at Atlantis massif, 30°N (Mid AtlanticRidge). Epitome 1 (Geoitalia 2005): 24.

Cannat M., Chatin F., Whitechurch H. and Ceuleneer G., 1997. Gabbroic rocks trapped in the upper mantle at the Mid-Atlantic ridge. In: J.A. Karson, M. Cannat, D.J. Miller and D. Elthon (Eds.), Proceed. O.D.P., Sci. Res., 153: 243-264.

Carbone S. and Lentini F., 1981. Caratteri deposizionali delle vulcaniti del Miocene Superiore negli Iblei (Sicilia sud-orientale). Geol. Romana, 20: 79-101.

Cortesogno L. and Lucchetti G., 1984. Ocean-floor metamorphism of the volcanic and sedimentary sequences in the Northern Apennine ophiolites: mineralogical and paragenetic features. Ofioliti, 9 (3): 363-400.

D’Antonio M. and Kristensen M. B., 2005. Hydrothermal alteration of oceanic crust in the West Philippine Sea basin (Ocean Drilling Program leg 195, Site 1201): inferences from a mineral chemistry investigation. Mineral. Petrol., 83: 87-112

Della Vedova B., Pellis G. and Pinna E., 1989. Studio geofisico dell’area di transizione tra il Mar Pelagico e la piana abissale dello Jonio. Atti 8° Convegno GNGTS, p. 543-558.

Dubinska E., Bylina P., Kozlowski A., Dörr W., Nejbert K., Scastock J. and Kulicki C., 2004. U-Pb dating of serpentinization: hydrothermal zircon from a metasomatic rodingite shell (Sudetic Ophiolite, SW Poland). Chem. Geol., 203: 183-203.

Fulignati P., Malfitano G. and Sbrana A., 1997. The Pantelleria caldera geothermal system: data from the hydrothermal minerals. J. Volcan. Geoth. Res., 75: 251-270.

Geisler T., Pidgeonm R.T., Van Bronswijkc W. and Kurtza R., 2002. Transport of uranium, thorium, and lead in metamict zircon under low-temperature hydrothermal conditions. Chem. Geol., 191: 141-154

Hoskin, P.W.O., 2005. Trace-element composition of hydrothermal zircon and the alteration of Hadean zircon from the Jack Hills, Australia. Geoch. Cosm. Acta. 69 (3): 637-648.

Hoskin P.W.O., Kinny P.D. and Wyborn D., 1998. Chemistry of hydrothermal zircon: investigating timing and nature of water-rock interaction. In: G.B. Arehart and J.R. Hulston (Eds.), Proceed. 9th Intern. Symp. "Water-rock interaction", Balkema/Rotterdam/Brookfield, Taupo New Zealand, p. 545-548.

Kerrich R. and Kyser T.K., 1994. 100 MA timing paradox of archean Gold, Abitibi Greenstone Belt (Canada) - New evidence from U-Pb and Pb-Pb evaporation ages of hydrothermal zircons. Geology, 22 (12): 1131-1134.

Kretz R., 1983. Symbols for rock-forming minerals. Am. Mineral., 68: 277-279.

Lassiter J.C., Hauri E.H., Nikogosian I.K. and Barsczus H.G., 2002. Chlorine/Potassium variations in melt inclusions from Raivavae and Rapa, Austral Islands: constraints on chlorine recycling in the mantle and evidence for brine-induced melting of oceanic crust. Earth Planet. Sci. Lett., 202: 525-540.

Natland J.H. and Dick H.J.B., 2001. Formation of the lower ocean crust and the crystallization of gabbroic cumulates at a very slowly spreading ridge. J. Volcan. Geotherm. Res., 110: 191-233.

Palandri J.L. and Reed M., 2003. Geochemical models of metasomatism in ultramafic systems: serpentinization, rodingitization, and sea floor carbonate chimney precipitation. Geoch. Cosm. Acta, 68: 1115-1133.

Pettke T., Audétat A., Schaltegger U. and Heinrich C. A., 2005. Magmatic-to-hydrothermal crystallization in the W-Sn mineralized Mole Granite (NSW, Australia): Part II: evolving zircon and thorite trace element chemistry. Chem. Geol., 220: 191-213.

Plank T. and Langmuir C.H., 1998. The chemical composition of subducting sediment and its consequences for the crust and mantle. Chem. Geol., 145 (3-4): 325-394.

Punturo R., Kern H., Scribano V. and Atzori P., 2000. Petrophysical and petrological characteristics of deep-seated xenoliths from Hyblean Plateau, South-Eastern Sicily, Italy: suggestions for a lithospheric model. Mineral. Petrogr. Acta, 43: 1-20.

Robinson D., Schmidt S. Th. and Santana De Zamora A., 2002. Reaction pathways and reaction progress for the smectite-to-chlorite transformation: evidence from hydrothermally altered metabasites. J. Metam. Geol., 20: 167-174.

Rubin J.N., Henry C.D. and Price J.G., 1993. The mobility of zirconium and other "immobile" elements during hydrothermal alteration. Chem. Geol., 110 (1-3): 29-47.

Salvi S. and Williams-Jones A.E., 1996. The role of hydrothermal processes in concentrating high-field strenght elements in the Strange Lake peralkaline complex, northeastern Canada. Geoch. Cosm. Acta, 60: 1917-1932.

Sapienza G.T., Griffin W.L., O'Reilly S.Y., Morten L. and Scribano V., 2005a. U-Pb ages and Hf isotope composition of zircons in a metasomatic xenolith (Hyblean Plateau, SE Sicily). Epitome, 1 (Geoitalia 2005): 129.

Sapienza G.T., Griffin W.L., O'Reilly S.Y., Morten L., Scribano V. and Braga R., 2005b. Morphological and trace element study of zircons from a metasomatic xenolith (Hyblean Plateau, SE Sicily). Epitome 1 (Geoitalia 2005): 141.

Sapienza G. and Scribano V., 2000. Distribution and representative whole-rock chemistry of deep-seated xenoliths from the Iblean Plateau, South-Eastern Sicily, Italy. Period. Mineral., 69: 185-204.

Schminke H.-U., Behncke B., Grasso M. and Raffi S., 1997. Evolution of the Northwestern Iblean Mountains, Sicily: uplift, Pliocene/Pleistocene sea-level changes, palaeoenvironment, and volcanism. Geol. Rundsch., 86: 637-669.

Scribano V., 1987. The ultramafic and mafic nodule suite in a tuff-breccia pipe from Cozzo Molino (Hyblean Plateau, SE Sicily). Rend. S.I.M.P., 42: 203-217.

Scribano V., Ioppolo S., Sapienza G. and Calvari S., 2003. Ipotesi sull'origine dei feldispati alcalini di alcuni xenoliti crostali degli Iblei. Boll. Accad. Gioenia Sci. Nat., Catania, 36: 5-21

Scribano V., Sapienza G., Braga R., and Morten L., 2006. Gabbroic xenoliths in tuff-breccia pipes from the Hyblean Plateau: insights into the nature and composition of the lower crust underneath South-Eastern Sicily, Italy. Mineral. Petrol., 86: 63-88

Tonarini S., D'Orazio M., Armenti P., Innocenti F. and Scribano V., 1996. Geochemical features of Eastern Sicily lithosphere as probed by Hyblean xenoliths and lavas. Eur. J Mineral., 8: 1153-1173.

Trua T., Esperança S. and Mazzuoli R., 1998. The evolution of the lithospheric mantle along the N. African plate: geochemical and isotopic evidence from the tholeiitic and alkaline volcanic rocks of the Hyblean Plateau, Italy. Contrib. Mineral. Petrol., 131: 307-322.

Received, February 25, 2006
Accepted, November 4, 2006